Acta Oceanol. Sin., 2015, Vol. 34, No. 1, P. 55–65
DOI: 10.1007/s13131-015-0596-9
http://www.hyxb.org.cn
E-mail: hyxbe@263.net

The El Niño-Southern Oscillation cycle simulated by the climate system model of Chinese Academy of Sciences

SU Tonghua[1,2], XUE Feng[1]*, SUN Hongchuan[3], ZHOU Guangqing[1]

[1] International Center for Climate and Environment Sciences, Institute of Atmospheric Physics, Chinese Academy of Sciences, Beijing 100029, China
[2] Fujian Meteorological Observatory, Fuzhou 350001, China
[3] Jiangsu Meteorological Observatory, Nanjing 210009, China

Received 7 April 2014; accepted 10 September 2014

Abstract

On the basis of more than 200-year control run, the performance of the climate system model of Chinese Academy of Sciences (CAS-ESM-C) in simulating the El Niño-Southern Oscillation (ENSO) cycle is evaluated, including the onset, development and decay of the ENSO. It is shown that, the model can reasonably simulate the annual cycle and interannual variability of sea surface temperature (SST) in the tropical Pacific, as well as the seasonal phase-locking of the ENSO. The model also captures two prerequisites for the El Niño onset, i.e., a westerly anomaly and a warm SST anomaly in the equatorial western Pacific. Owing to too strong forcing from an extratropical meridional wind, however, the westerly anomaly in this region is largely overestimated. Moreover, the simulated thermocline is much shallower with a weaker slope. As a result, the warm SST anomaly from the western Pacific propagates eastward more quickly, leading to a faster development of an El Niño. During the decay stage, owing to a stronger El Niño in the model, the secondary Gill-type response of the tropical atmosphere to the eastern Pacific warming is much stronger, thereby resulting in a persistent easterly anomaly in the western Pacific. Meanwhile, a cold anomaly in the warm pool appears as a result of a lifted thermocline via Ekman pumping. Finally, an El Niño decays into a La Niña through their interactions. In addition, the shorter period and larger amplitude of the ENSO in the model can be attributed to a shallower thermocline in the equatorial Pacific, which speeds up the zonal redistribution of a heat content in the upper ocean.

Key words: climate system model of Chinese Academy of Sciences, El Niño-Southern Oscillation cycle, El Niño, thermocline, wind stress

Citation: Su Tonghua, Xue Feng, Sun Hongchuan, Zhou Guangqing. 2015. The El Niño-Southern Oscillation cycle simulated by the climate system model of Chinese Academy of Sciences. Acta Oceanologica Sinica, 34(1): 55–65, doi: 10.1007/s13131-015-0596-9

1 Introduction

The El Niño-Southern Oscillation (ENSO) originates from air-sea interaction in the tropical Pacific (Bjerknes, 1969), with the oceanic component named El Niño and the atmospheric component named the Southern Oscillation. The interannual variation of the ENSO is quasi-periodic, appearing every 3–7 years. The warm phase and cold phase of the ENSO cycle, known as El Niño and La Niña, are characterized by a positive and negative sea surface temperature (SST) anomaly in the tropical central and eastern Pacific, respectively (Philander, 1985). Usually, the ENSO tends to be phase-locked with the annual cycle. It onsets in spring, reaching its peak in winter, finally decaying in the following summer (Rasmusson and Carpenter, 1982). In addition, an El Niño always shows a stronger anomaly and a more significant influence than a La Niña (Larkin and Harrison, 2002; An and Jin, 2004; Wu et al., 2010).

So far, several conceptual models have been proposed to reveal the mechanisms for the phase transition of the ENSO, such as the trade wind relaxation (Wyrtki, 1975), the delayed action oscillator (Suarez and Scorf, 1988), the equatorial recharge paradigm (Jin, 1997), the western Pacific oscillator (Weisberg and Wang, 1997), and the advective-reflective model (Picaut et al., 1997). Although some deductions based on the delayed action oscillator have not been observed, it is widely accepted because it can explain most of the observed features. The other three paradigms are all derived from this model.

It has been shown that, there are two prerequisites for the occurrence of an El Niño, i. e., a westerly anomaly and a subsurface temperature anomaly in the western equatorial Pacific (e. g., Li and Mu, 1999; Xue and He, 2007; Liu and Xue, 2012). With a burst of the westerly anomaly in the western Pacific, a warm Kelvin wave starts to propagate eastward along the thermocline, leading to the occurrence of a positive SST anomaly in the tropical eastern Pacific. Through the Bjerknes positive feedback, an El Niño further develops and reaches its peak (Jin, 1997). While all the theoretical models are essentially the same in explaining the development of an El Niño, there are basic differences in interpreting the transition process (Liu and Xue, 2010a, b). In particular, different aspects are emphasized in these models, i.e., the reflection of the oceanic waves in the delayed action oscillator, the reduction of the heat content caused by a Sverdrup divergence in the equatorial recharge paradigm,

Foundation item: The Strategic Priority Research Program of Chinese Academy of Sciences under contract No. XDA05110201; the National Basic Research Program (973 Program) of China under contract No. 2010CB951901.
*Corresponding author, E-mail: fxue@lasg.iap.ac.cn

the easterly anomaly induced by the tropical western Pacific anticyclone in the western Pacific oscillator, and the advection and reflection of the oceanic waves in the advective-reflective model.

Although the ENSO cycle is a self-sustaining oscillating mode in the tropical air-sea coupling system (Philander and Fedorov, 2003), there exhibits a strong nonlinearity in its intensity, decay and impact (Xue and Liu, 2008; Liu and Xue, 2008; Liu and Xue, 2010a, b). In addition, a random disturbance plays a role in the occurrence of an ENSO event (Philander, 1983). More comprehensively, the ENSO cycle is a product resulting from the interactions at various spatio-temporal scales. Therefore, a numerical model with fine physical processes is an essential tool for understanding and predicting the ENSO.

From the early simplified Zebiak-Cane model (Zebiak and Cane, 1987) to the complex atmosphere-land-ocean-ice fully-coupled models, there have been great improvements in the simulation and prediction of the ENSO. Owing to imperfect physical processes, however, there exist notable biases in ENSO simulation. On the basis of the results from the El Niño simulation intercomparison project (ENSIP) and phase 3 of the coupled model intercomparison project (CMIP3), some biases in the ENSO simulation were identified, i.e., a weak seasonal phase-locking (Latif et al., 2001; AchutaRao and Sperber, 2006), a shorter periodicity (Guilyardi, 2006; Guilyardi et al., 2009), a stronger amplitude (Yu and Kim, 2010) and too far westward extension of the equatorial cold tongue (Leloup et al., 2008). Although the latest CMIP5 models showed an improvement in the equatorial cold tongue and amplitude, a variety of feedback mechanisms for the ENSO cycle have remained to be resolved (Bellenger et al., 2014).

Since the early 1990s, a series of air-sea coupled models have been developed in the Institute of Atmospheric Physics (IAP), Chinese Academy of Sciences (CAS), and these models were successfully used to simulate and predict the ENSO (Zhou and Li, 1999; Zhou et al., 1999). Recently, a new generation climate system model (hereafter referred to the CAS-ESM-C) was developed with a higher resolution and more complete physical processes (Sun et al., 2012). On the basis of a long-term integration of the model, this study aims at evaluating its performance in simulating the ENSO cycle, with a focus on the development and decay of an El Niño. The reminder of this paper is organized as follows: Section 2 describes the model, experiment design and observational data; the basic features of the simulated ENSO cycle are shown in Section 3; in Section 4, we evaluate the model's performance in the development and decay of an El Niño; the model's bias is discussed in Section 5; and a summary is given in the last section.

2 Model, experiment and observational data

2.1 *model and experiment*

The climate system model of Chinese Academy of Sciences is an atmosphere-ocean-land-ice fully coupled model with a modular structure (Sun et al., 2012). The four components in the model are coupled through the Coupler-6, which was introduced from the National Center for Atmospheric Research (NCAR). The atmospheric component is the fourth generation atmospheric general circulation model (IAP AGCM4.0) developed at the IAP, with a horizontal resolution of 1.4°×1.4° and 26 vertical layers (Zhang, 2009). The oceanic component is the LICOM1.0, with a horizontal resolution of 1.0°×1.0° and 30 vertical layers (Liu et al., 2004). Besides, the land surface and sea ice components are the NCAR CLM3.0 and CSIM5, respectively (Dickinson et al., 2006; Briegleb et al., 2004).

The model results used here are the pre-industrial control integration. All the external forcing values are set to the level in 1850, when a solar radiation constant is 1 365 W/m², and greenhouse gas mixing ratios (including CO_2, CH_4, N_2O) are 284×10^{-6}, 790×10^{-12}, and 275×10^{-12}, respectively. For the integration of atmosphere-land coupled model, the instantaneous fields on January 1st of the 20th year are taken as the initial fields in the atmosphere model and the land surface model, respectively. The initial fields in the ocean model are set to December 31st of the 2000th year in a 2000-year spin-up. There is no spin-up process for the sea ice model. The model has been run for 227 years. It was shown that, after 20 years integration, the SST tends to be fluctuated with no significant upward or downward trend, indicating that the model reaches an equilibrium state (Sun et al., 2012). Therefore, the model results from the 28th year to 227th year are used and the model climate is based on the 200-year mean.

2.2 *Observational data*

To evaluate the model's performance, various observational data are employed: (1) SST dataset from Hadley Center with a horizontal resolution of 1.0°×1.0° (Rayner et al., 2003); (2) EN3 subsurface sea temperature with a resolution of 1.0°×1.0° and 30 vertical layers (Ingleby and Huddleston, 2007); (3) the second version of the daily reanalysis product taken from the National Centers for Environmental Prediction (NCEP) with a horizontal resolution of 2.5°×2.5° and 17 vertical layers (Kanamitsu et al., 2002); (4) outgoing long-wave radiation (OLR) derived from satellite observations of the National Oceanic and Atmospheric Administration (NOAA) with a resolution of 2.5°×2.5° (Liebmann and Smith, 1996); and (5) reanalysis product of the simple ocean data assimilation (SODA) developed in the University of Maryland with a resolution of 0.5°×0.5° (Carton et al., 2000). All of the datasets cover the period from 1979 to 2012. In addition, the seasonal mean in winter or summer is obtained from the 3-month mean during December-January-February or June-July-August.

3 Basic features of the ENSO cycle

Figure 1 shows the observed and simulated standard deviations of the tropical Pacific SST in winter and summer. The maxima in winter are located in the tropical eastern Pacific, with a largest value over 1.4°C (Fig. 1a). In summer, the maximum is greatly reduced and confined to the southeastern Pacific (Fig. 1b). There exhibits a robust annual cycle of the interannual variability in the tropical eastern Pacific. In general, the model simulates the observed maxima in the tropical eastern Pacific and its annual cycle (Figs 1c and d). However, there exist some biases in the model. The simulated maxima are overly confined to the equatorial regions, and the standard deviation is much larger than the observation, with the maximum greater than 2°C. Because the interannual variability of the tropical Pacific SST reflects the zonal redistribution of heat and mass in the upper ocean, a larger standard deviation in the tropical central and eastern Pacific will result in a smaller one in other regions of the Pacific, especially in winter (Figs 1c and d).

On the basis of the method proposed by Trenberth (1997), the SST anomaly in Niño3.4 region (5°S–5°N, 170°–120°W) is used to describe the ENSO activity (hereafter referred to Niño3.4 index). As shown in Fig. 2, the observation exhibits a strong power between 2 and 7 years, particularly between 3 and

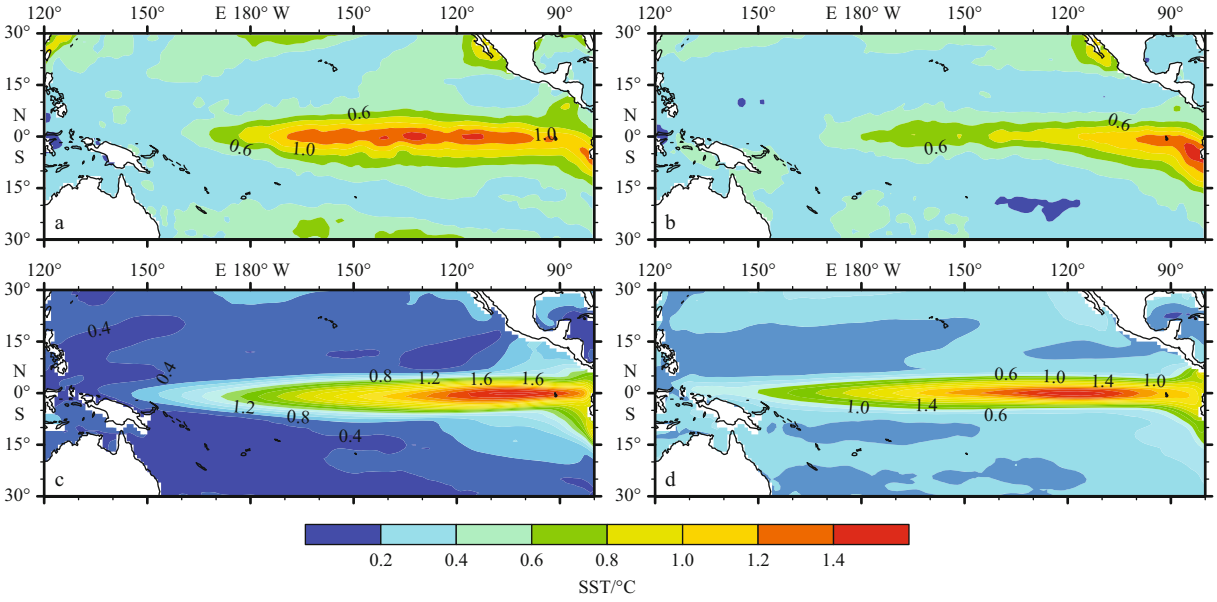

Fig. 1. The observed (a and b) and simulated (c and d) standard deviation of the sea surface temperature (°C) in the tropical Pacific in boreal winter (a and c) and boreal summer (b and d).

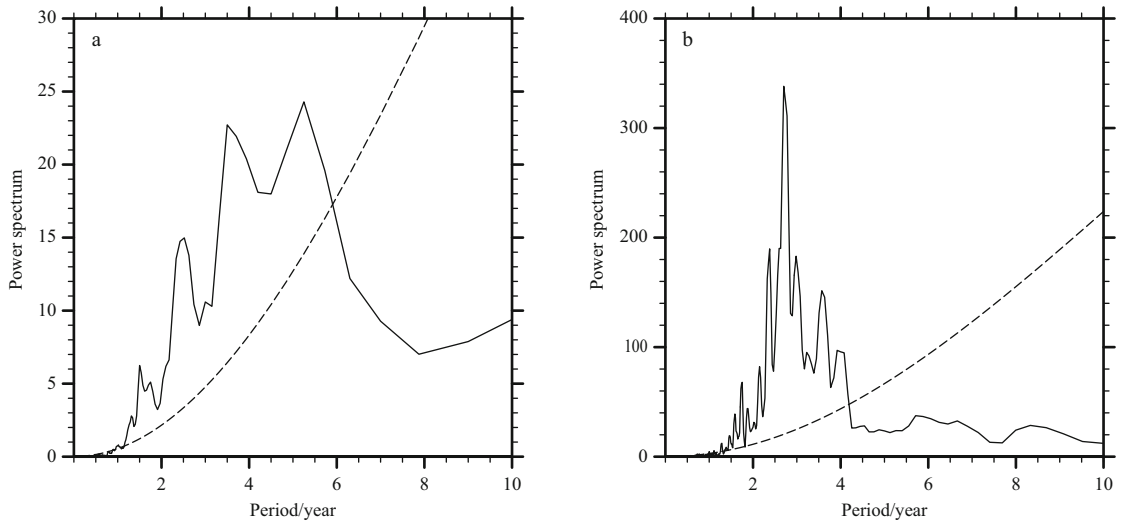

Fig. 2. The observed (a) and simulated (b) power spectra of the Niño3.4 index. The dashed line indicates the 0.95 confidence level for the red noise spectrum.

5 years. Instead, the simulated powers are more significant between 2 and 5 years, with a peak of 3 years. The period of the ENSO in the model is shorter than the observation. It is also noted that, the simulated peak power is much stronger than the observation due to a higher frequency and stronger amplitude of the ENSO.

When 3 month running-mean SST anomaly in the Niño3.4 region is greater than or equal to 0.5°C within 5 consecutive months, an El Niño event can be identified (Trenberth, 1997). During the period of 1979–2012, nine El Niño events are thus identified, i.e., 1982–1983, 1986–1988, 1991–1992, 1994–1995, 1997–1998, 2002–2003, 2004–2005, 2006–2007, 2009–2010, respectively. It should be pointed out that, since the El Niño event during 1986–1988 is not phase-locked to the annual cycle (Liu and Xue, 2010a), this event is excluded in the following composite analysis. In addition, since the simulated stand deviation in the Niño3.4 region is nearly twice as the observation (Fig. 1), the critical value for identifying El Niño events in the model is deliberately set to 1.0°C instead of 0.5°C in the observation. Accordingly, 70 El Niño events are identified in the model.

Figure 3 shows the observed and simulated El Niño events. The El Niño developing year (the decaying year) is marked with "0" ("+1") respectively. Usually, the composite Niño3.4 index (indicated by the red line) becomes positive in April of Year 0, then increasing rapidly during the two consecutive stages, reaching a peak around November and December. Afterwards, it decays quickly with a negative value in June of Year +1, finally turning into a La Niña event (Fig. 3a). The model generally simulates the above observed features, but the simulated El Niño tends to develop more rapidly, reaching its peak in September with 2 or 3 months earlier than the observation. By contrast, the decaying process agrees well with the observation. Thus a

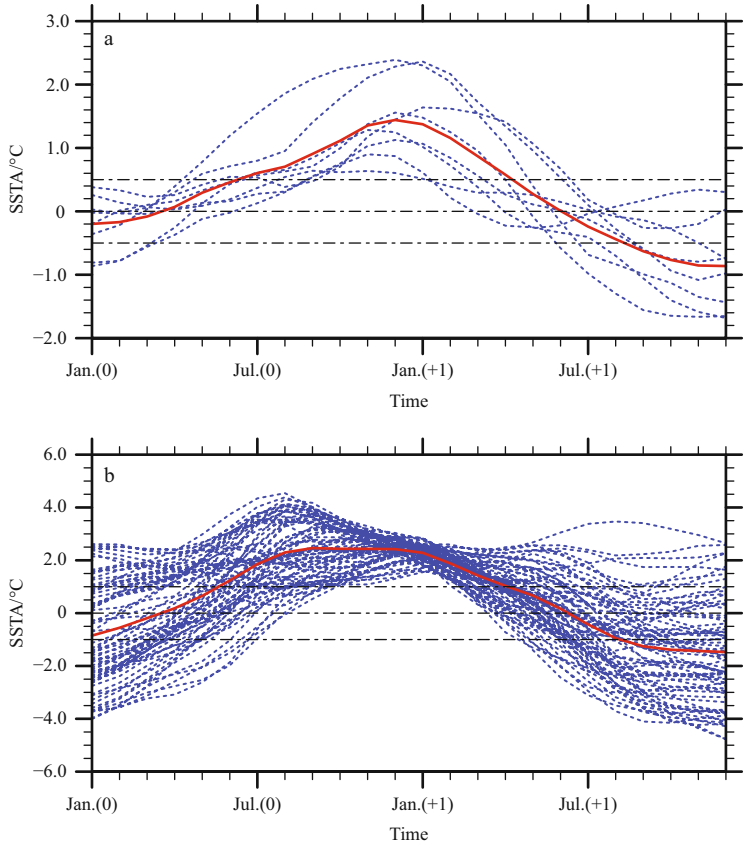

Fig. 3. The observed (a) and simulated (b) time series of SST anomaly over the Niño3.4 region. The "0" and "+1" in the abscissa represent the developing and decaying years of El Niño, respectively. The dashed blue lines indicate the individual El Niño events and the solid red lines indicate the composite of all El Niño events.

longer time for the El Niño peak phase is found in the model. Besides, much stronger amplitude of 4°C is found in the model instead of 2°C in the observation.

Although the El Niño intensity in the model is generally overestimated, the intensity of each event can still be distinguished. Clearly, the El Niño events with different intensity decay into a different state. Statistically, about 60% of the simulated El Niño events decay into a La Niña event, and 29% decay into a normal state. Therefore, the composite results actually reflect the signal of strong El Niño events. This fact indicates that, the nonlinear relationship between the El Niño intensity and its decaying result revealed by Liu and Xue (2010a, b) is also reproduced by the model.

4 The ENSO cycle

4.1 *Occurrence and development of an El Niño*

It has been revealed that a positive subsurface heat content anomaly in the western tropical Pacific is one of prerequisites for the occurrence of an El Niño. In general, there appears a robust anomaly 6 months to 2 years before an El Niño occurs (Li and Mu, 1999; Zhou et al., 1999; Liu and Xue, 2012). Figure 4 shows the depth-longitude cross-section of the subsurface temperature anomaly. In January of Year 0 (Fig. 4a), a positive anomaly appears in the western equatorial Pacific, and its maximum extends eastward to the dateline. Afterwards, the warm anomaly further propagates eastward (Fig. 4c). By July, the equatorial eastern Pacific is occupied by a positive SST anomaly with an average value greater than 0.5°C (Fig. 4e), signaling the occurrence of an El Niño. In October of Year 0 (Fig. 4g), the anomaly continues to develop locally in the eastern Pacific, and reaches a peak in winter (Fig. 4i). The model generally simulates the eastward propagating process, but it overestimates the propagating speed with a shallower anomaly than the observation (Figs 4b, d, f, and h). As shown in Fig. 4f, when an El Niño occurs, the simulated maximum has arrived at 120°W instead of 130°W in the observation (Fig. 4e).

The maintenance of the equatorial westerly anomaly is also necessary for the occurrence of an El Niño (Liu and Xue, 2012). By exciting a warm Kelvin wave, it pushes the accumulated warm water in the western Pacific to propagate eastward along the subsurface. As shown in Fig. 5a, prior to the occurrence of an El Niño, there exhibit twice enhancements of the westerly anomaly in the tropical western Pacific in spring and summer, respectively. Compared with the observation, the model fails to simulate the enhancing process in a stepwise manner (Fig. 5b). Instead, the westerly anomaly in the model tends to intensify very rapidly from April of Year 0, and then propagates eastward faster than the observation. As a result, the subsurface anomaly also propagates faster (Fig. 4).

It was revealed that, the westerly anomaly in the tropical western Pacific can be attributed to the boundary forcing and the air-sea interaction, but they play a different role at different stages (Liu and Xue, 2008). In spring, a weak anti-Walker circulation arising from the Bjerknes positive feedback is found due to a weak warming in the eastern Pacific. Therefore, the meridional forcing from the extratropics is more important to the burst of the equatorial westerly anomaly. In both observation

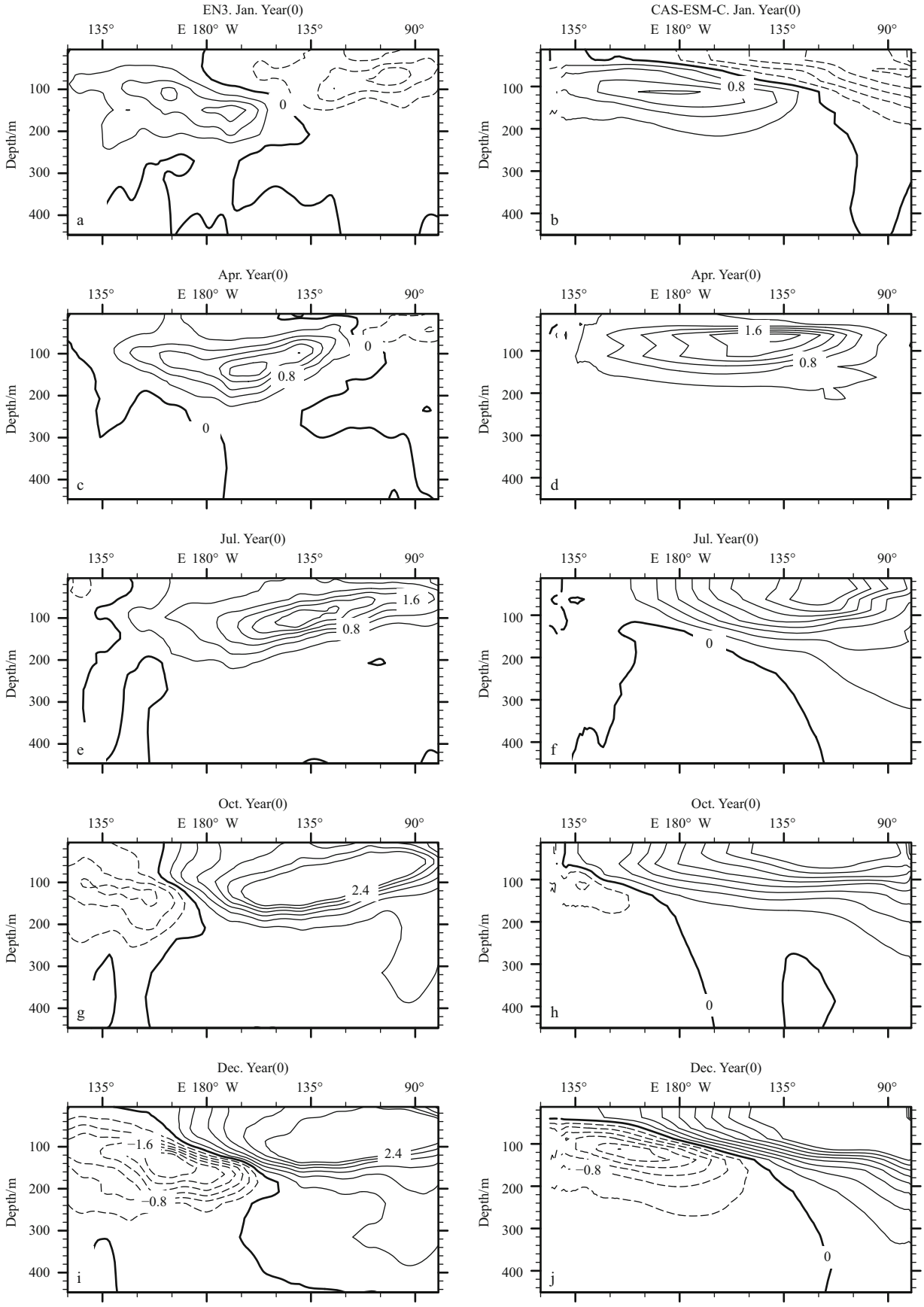

Fig. 4. The depth-longitude cross-sections of the composite subsurface ocean temperature (°C) along the equator in January (a and b), April (c and d), July (e and f), October (g and h), and December (i and j) of the El Niño developing year.

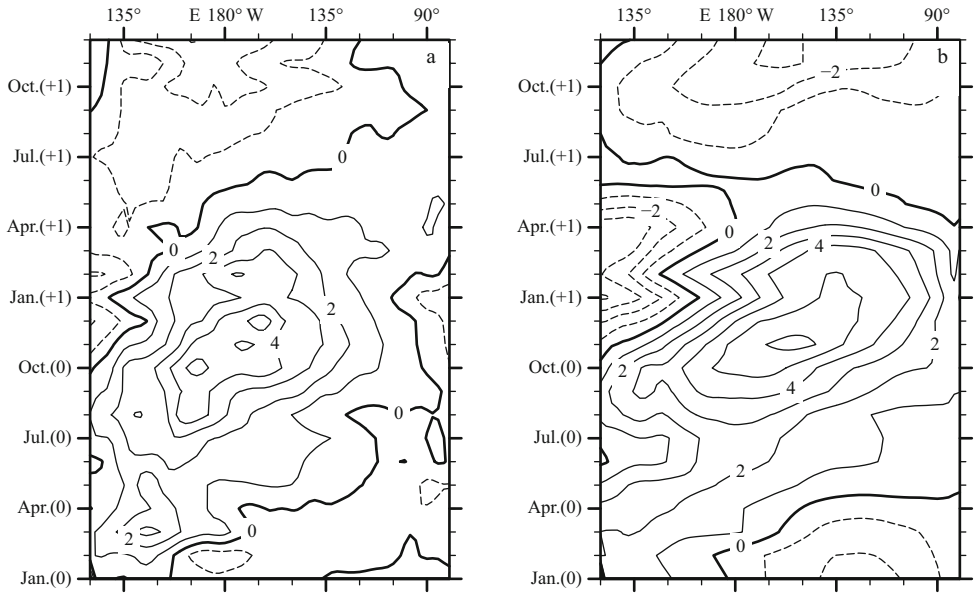

Fig. 5. The time-longitude cross-sections of the composite zonal wind (m/s) along the equator in the observation (a) and simulation (b). The "0" and "+1" in the vertical coordinates represent the developing and decaying years of El Niño, respectively.

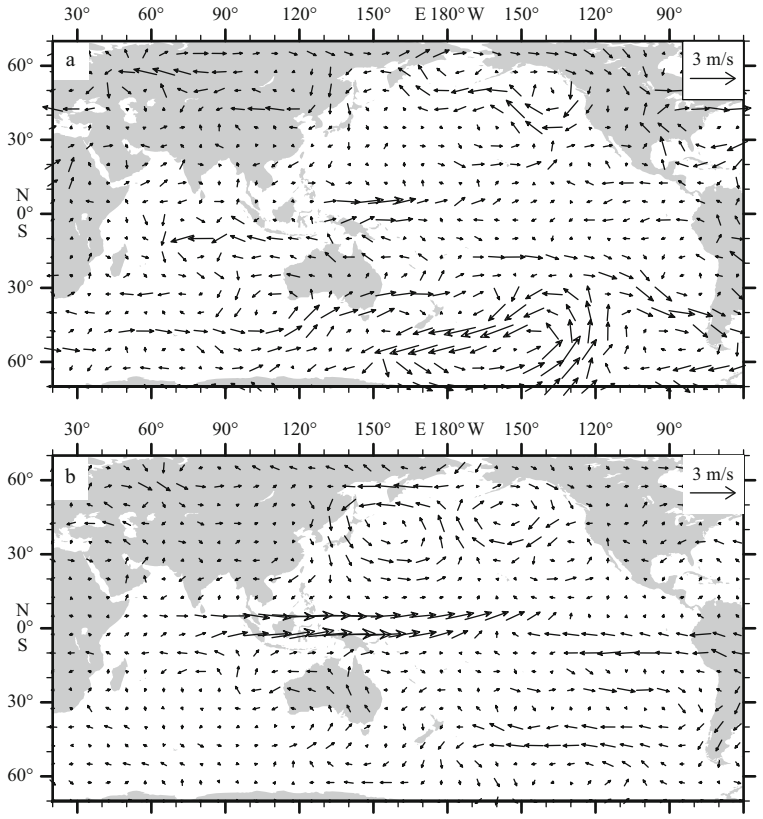

Fig. 6. The observed (a) and simulated (b) composite 850 hPa wind fields (m/s) in April of the El Niño developing year.

and simulation, a meridional wind anomaly is evident in both hemispheres (Fig. 6). In the model, however, a much stronger cyclonic anomaly is found in the tropical northwestern Pacific (Fig. 6b), resulting in too strong meridional forcing and westerly anomaly in the equatorial Pacific. Accordingly, the simulated El Niño tends to develop faster due to a faster eastward propagation of the warm anomaly and the intensified Bjerknes positive feedback in the tropical Pacific.

4.2 *Decay of an El Niño*

Similar to the development, the decaying process of an El Niño is also related to the eastward propagation of the negative anomaly in the western Pacific (Liu and Xue, 2010a, b). As shown in Fig. 7a, when an El Niño reaches a peak, a significant

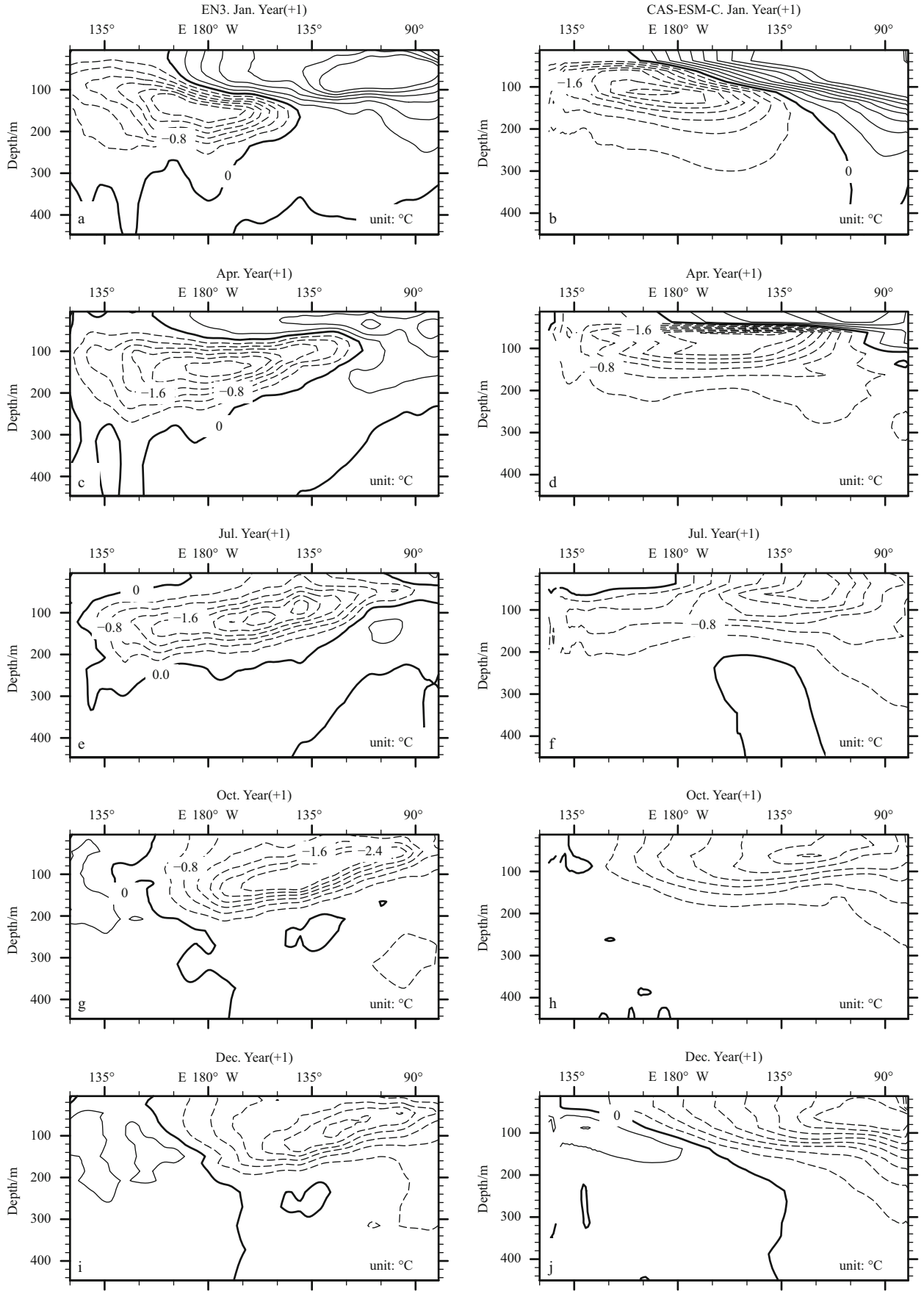

Fig. 7. The same as Fig. 4, but for the El Niño decaying year.

negative anomaly appears in the western equatorial Pacific. Meanwhile, due to a Gill-type response to the SST warming in the eastern equatorial Pacific, a pair of the cyclonic wind stress anomalies is found in the central Pacific (Fig. 8a). With a lift of the thermocline via Ekman pumping, the local convection is suppressed due to a reduced local SST. Through a secondary Gill-type response (Fig. 8a) (Liu and Xue, 2010a), there appears an anomalous anticyclone in the tropical northwestern Pacific along with an easterly anomaly to the south.

Owing to a local air-sea interaction, the anomalous anticyclone maintains for a long time, and it propagates eastward slowly, leading to a persistent propagation of the easterly anomaly (Fig. 5a). As a result, a cold Kelvin wave is excited on the subsurface, and the cold anomaly propagates eastward from the western Pacific to the eastern Pacific (Figs 7c, e, and g). This process is well simulated by the model although with a relatively flatter signal (Figs 7b, d, f, and h). Besides, the simulated decaying speed is close to the observation, as also seen in Fig. 3. This is different from the developing process as mentioned above.

The above decaying process is similar to the western Pacific oscillator theory (Weisberg and Wang, 1997), in which the mechanism for the phase transition is only effective for a strong El Niño. For a moderate El Niño, however, the mechanism fails to work after the peak phase. As a result, the moderate El Niño tends to restore to a normal state in the eastern Pacific (Liu and Xue, 2010b). Owing to an overestimated intensity, the mechanism is particularly important to the phase transition in the model.

5 Discussion

On the basis of a simple coupled ocean-atmosphere model, Fedorov and Philander (2001) found that there are two types of unstable modes in the tropical ocean-atmosphere coupling system. With a deeper thermocline, one mode possesses a longer period of several years. Instead, a shorter period of about 2 years is found in the other mode, which requires a shallower thermocline. Furthermore, the period and the amplitude of the ENSO are closely related to the climate state in the tropical Pacific, especially the thermocline (Guilyardi, 2006).

Figure 9 shows the climatological mean subsurface temperature in different seasons. A much shallower thermocline is simulated by the model in the equatorial Pacific, especially in the warm pool region. As indicated by the 20°C isotherm, the observed thermocline is deeper than 150 m during all seasons. Instead, the thermocline in the model is only about 130 m. According to the delayed oscillator theory (Suarez and Schopf, 1988), a shallower thermocline will reduce the interval of the delayed feedback and speed up the wave propagation in the upper ocean. As a result, the subsurface heat content anomaly in the model propagates eastward faster, hence the El Niño events occur more frequently.

Also evident in Fig. 9 is a weaker slope of the thermocline in the model, which is corresponding to a weaker wind stress due

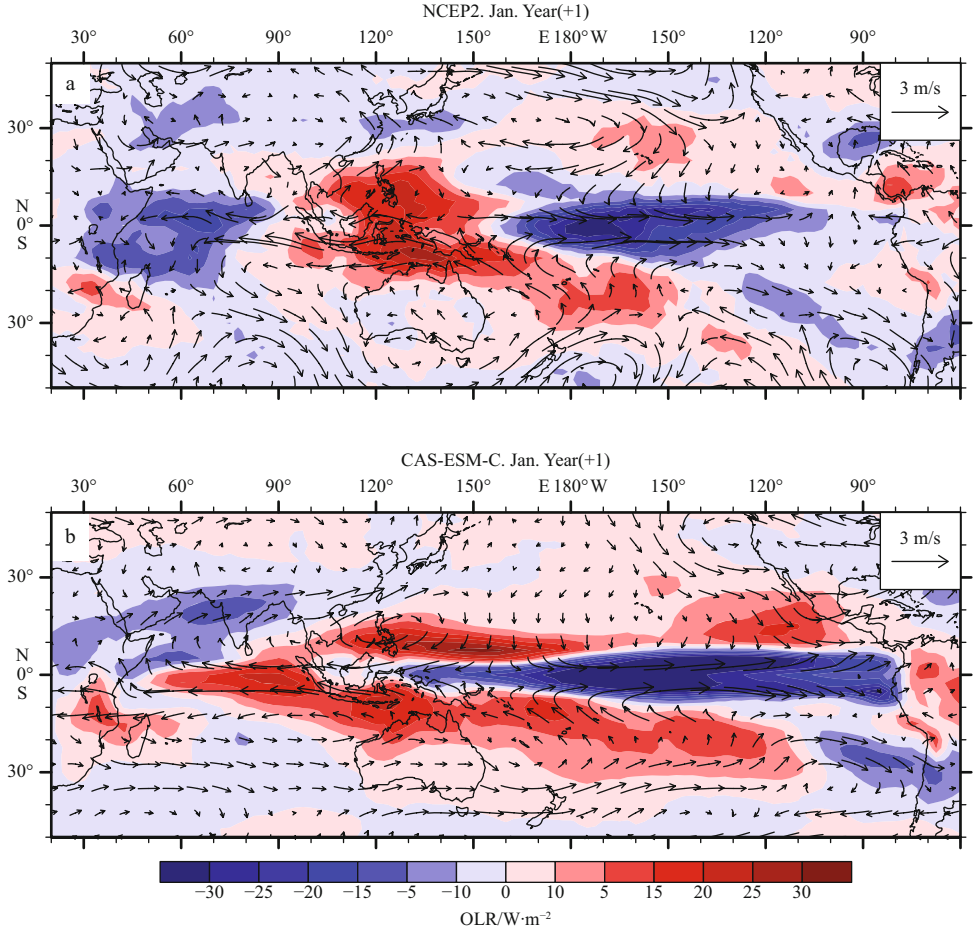

Fig. 8. The anomalous OLR fields (W/m^2) and 850 hPa wind fields (m/s) in January of the El Niño decaying year in the observation (a) and simulation (b).

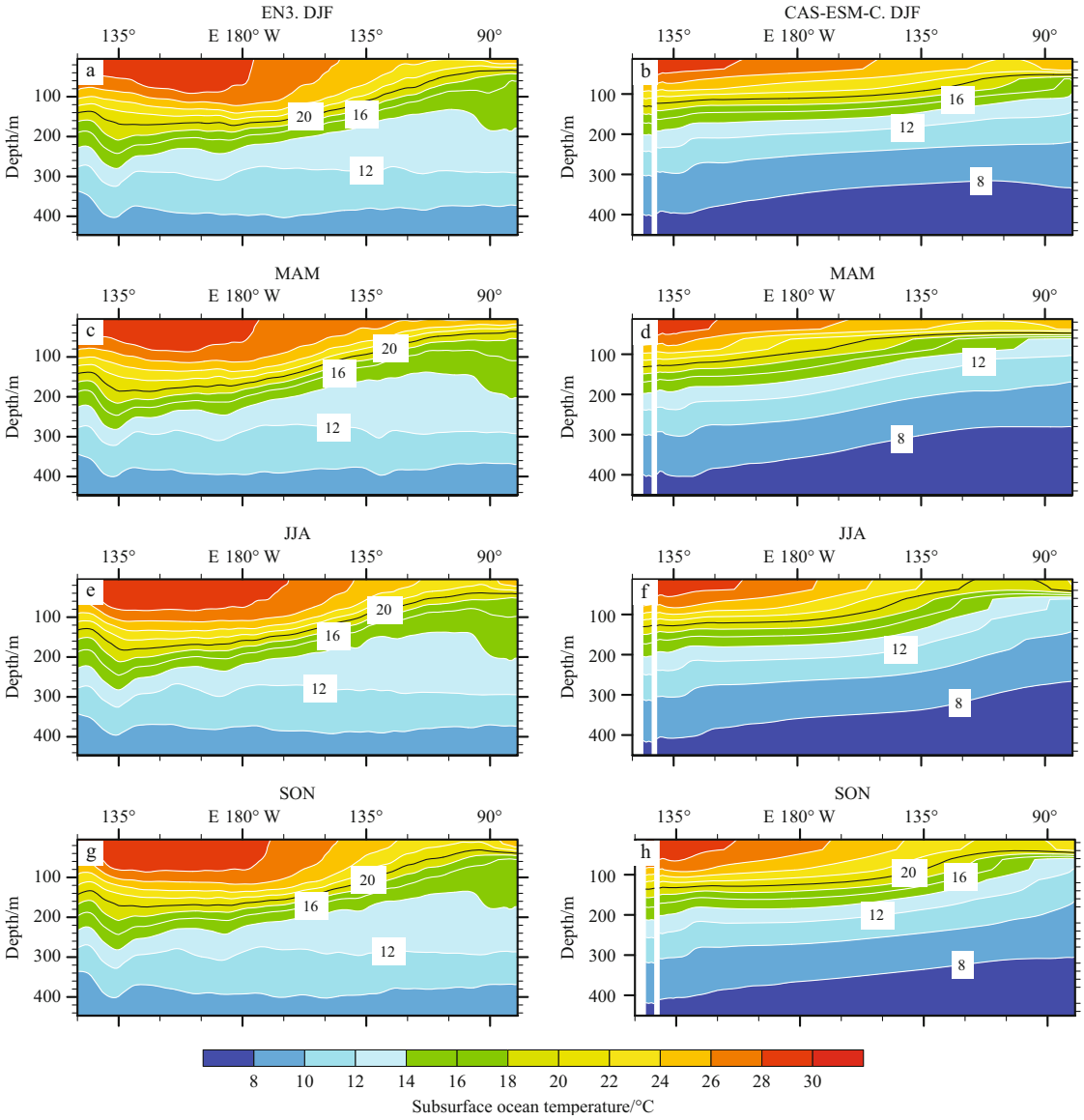

Fig. 9. The depth-longitude cross-section of the observed (left panels) and simulated (right panels) subsurface ocean temperature (°C) along the equator in winter (a, b), spring (c, d), summer (e, f), and autumn (g, h). The bold lines indicate the isotherm of 20°C, which can approximately represent the depth of thermocline.

to a balance between the tilt extent and the wind stress. As seen in Fig. 10a, an easterly wind (i.e., the trade wind) prevails in the equator all the year around. In the model, however, a weaker wind stress is simulated (Fig. 10b), as indicated by the westerly wind stress discrepancy (Fig. 10c). Accordingly, less warm water is accumulated in the western Pacific, and the thermocline in the eastern Pacific tends to be deepened. Consequently, more frequent El Niño events occur in the model due to a faster propagation of ocean waves along the thermocline with a weaker slope.

In fact, a shorter period of 2–3 years in the ENSO cycle is simulated by most of the early models participating the CMIP (AchutaRao and Sperber, 2006; Guilyardi et al., 2009). In CMIP5, more models tend to simulate a longer period owing to a better representation of the climatological mean SST and zonal wind stress in the equatorial Pacific (Bellenger et al., 2014). While the depth and slope of the thermocline in the wind-stress-driven ocean model are close to the observations (Liu et al., 2004), a weaker wind stress in the tropical Pacific is found in the SST-driven AGCM (Zhang, 2009). In the coupled model, the weaker wind stress can lead to a shallower thermocline, which in turn reduces the zonal pressure difference and exaggerates the bias in the wind stress in the tropical Pacific. Therefore, it is important to improve the wind stress in the atmospheric model for a better simulation of the ENSO period.

6 Conclusions

By using more than 200 years simulation of the climate system model of Chinese Academy of Sciences (CAS-ESM-C), we have evaluated the model performance in simulating the ENSO cycle, with a focus on the developing and decaying processes. The major conclusions are summarized as follows.

(1) The model generally simulates the annual cycle and interannual variability of the SST in the tropical Pacific. Besides, the model reproduces the phase-locking feature of an El Niño, i.e., onset in spring, peak in winter and decay in the following

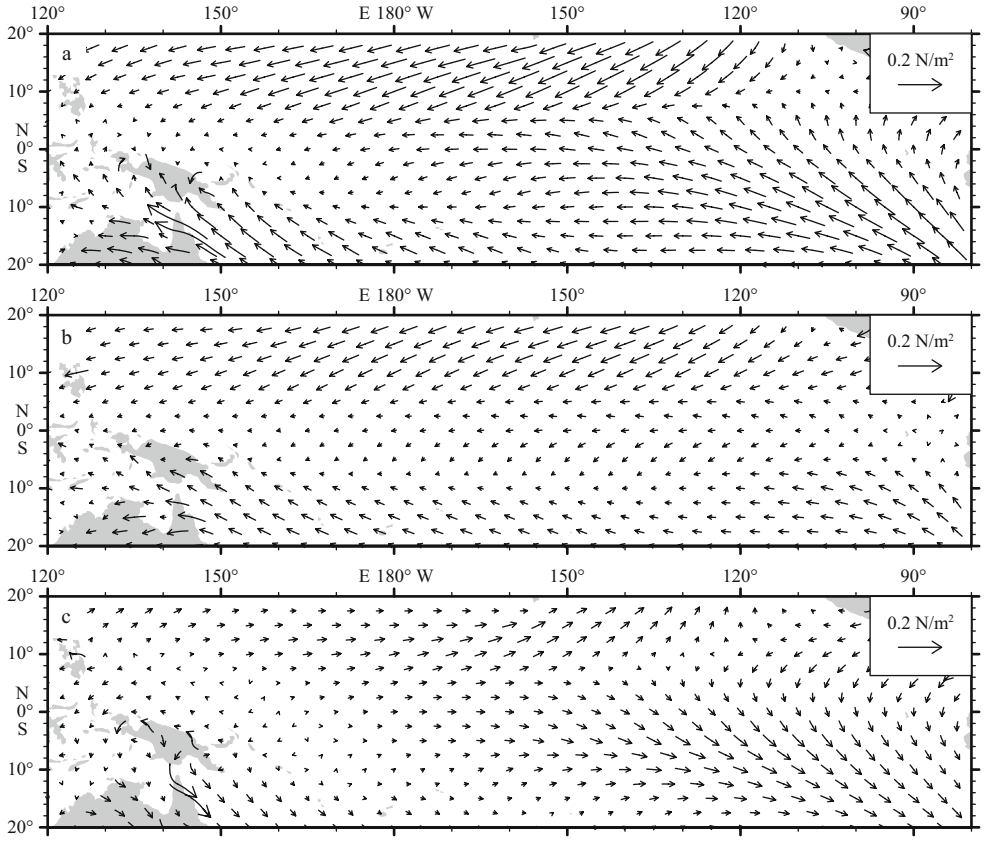

Fig. 10. The observed (a) and simulated (b) annual mean surface wind stress, and the difference between simulation and observation (c).

summer. Compared with the observation, however, the simulated ENSO exhibits a much stronger amplitude and shorter period of 2–3 years.

(2) The model reasonably simulates two prerequisites for the occurrence of an El Niño, i.e., the warm water accumulation and the westerly anomaly in the western equatorial Pacific. Owing to a stronger meridional forcing from the extratropics, the model overestimates the westerly anomaly in the equatorial western Pacific. Moreover, due to a shallower thermocline in the model, the El Niño tends to develop faster along with a faster eastward propagation of the subsurface warm anomaly.

(3) Owing to a secondary Gill-type response to the tropical eastern Pacific warming and a lifted thermocline via Ekman pumping, a cold water anomaly and an easterly anomaly are found in the western Pacific. This mechanism is only effective for a strong El Niño event. The response in the model occurs more frequently due to an overestimated intensity of the El Niño.

(4) A more frequent occurrence of the ENSO in the model is closely related to a shallower thermocline, which speeds up the zonal redistribution of the heat content in the upper Pacific Ocean. A further analysis shows that, the shallower thermocline can be attributed to the weaker wind stress in the equator. Therefore, it is necessary to improve the wind bias in the model.

References

AchutaRao K, Sperber K R. 2006. ENSO simulation in coupled ocean atmosphere models: are the current models better? Climate Dyn, 27(1): 1–15

An S I, Jin F F. 2004. Nonlinearity and asymmetry of ENSO. J Climate, 17(12): 2399–2412

Bellenger H, Guilyardi E, Leloup J, et al. 2014. ENSO representation in climate models: from CMIP3 to CMIP5. Climate Dyn, 42(7–8): 1999–2018

Bjerknes J. 1969. Atmospheric teleconnections from the equatorial Pacific. Mon Wea Rev, 97(3): 163–172

Briegleb B P, Bitz C M, Hunke E C, et al. 2004. Scientific description of the sea ice component in the community climate system model, version three. NCAR Technical Note NCAR/TN-463+STR, Colorado: National Center for Atmospheric Research, doi: 10.5065/D6HH6H1P.

Carton J A, Chepurin G, Cao X, et al. 2000. A simple ocean data assimilation analysis of the global upper ocean 1950-1995, Part 1: methodology. J Phys Oceanogr, 30(2): 294–309

Dickinson R E, Oleson K W, Bonan G, et al. 2006. The community land model and its climate statistics as a component of the community climate system model. J Climate, 19(11): 2302–2324

Fedorov A V, Philander S G. 2001. A stability analysis of tropical ocean-atmosphere interactions: Bridging measurements and theory for El Niño. J Climate, 14(14): 3086–3101

Guilyardi E. 2006. El Niño-mean state-seasonal cycle interactions in a multi-model ensemble. Climate Dyn, 26(4): 329–348

Guilyardi E, Wittenberg A, Fedorov A, et al. 2009. Understanding El Niño in ocean-atmosphere general circulation models: progress and challenges. Bull Amer Meteor Soc, 90(3): 325–340

Ingleby B, Huddleston M. 2007. Quality control of ocean temperature and salinity profiles-Historical and real-time data. J Marine Syst, 65(1–4): 158–175

Jin F F. 1997. An equatorial ocean recharge paradigm for ENSO. Part I: Conceptual model. J Atmos Sci, 54(7): 811–829

Kanamitsu M, Ebisuzaki W, Woollen J, et al. 2002. NCEP-DOE AMIP-II reanalysis (R-2). Bull Amer Meteor Soc, 83(11): 1631–1643

Larkin N K, Harrison D E. 2002. ENSO warm (El Niño) and cold (La Niña) event life cycles: Ocean surface anomaly patterns, their

symmetries, asymmetries, and implications. J Climate, 15(10): 1118–1140

Latif M, Sperber K, Arblaster J, et al. 2001. ENSIP: the El Niño simulation intercomparison project. Climate Dyn, 18(3–4): 255–276

Leloup J, Lengaigne M, Boulanger J P. 2008. Twentieth century ENSO characteristics in the IPCC database. Climate Dyn, 30(2–3): 277–291

Li Chongyin, Mu Mingquan. 1999. El Niño occurrence and sub-surface ocean temperature anomalies in the Pacific warm pool. Chinese Journal of Atmospheric Sciences (in Chinese), 23(5): 513–521

Liebmann B, Smith C A. 1996. Description of a complete (interpolated) outgoing longwave radiation dataset. Bull Amer Meteor Soc, 77: 1275–1277

Liu Changzheng, Xue Feng. 2008. The persistent maintenance of the strong westerly anomalies over the equatorial western Pacific during the onset and development of ENSO. Climatic and Environmental Research (in Chinese), 13(2): 161–170

Liu Changzheng, Xue Feng. 2010a. The decay of El Niño with different intensity. Part I, The decay of the strong El Niño. Chinese Journal of Geophysics, 53(1): 14–25

Liu Changzheng, Xue Feng. 2010b. The decay of El Niño with different intensity. Part II, The decay of the moderate and relatively-weak El Niño. Chinese Journal of Geophysics, 53(6): 915–925

Liu Changzheng, Xue Feng. 2012. The abortion of El Niño event in 1993 and its comparison with the typical El Niño event. Climatic and Environmental Research (in Chinese), 17(2): 197–204

Liu Hailong, Yu Yongqiang, Li Wei, et al. 2004. Manual for LASG/IAP Climate System Ocean Model (LICOM1.0) (in Chinese). Beijing: Science Press, 107

Philander S G H. 1983. El Niño and Southern Oscillation phenomena. Nature, 302(5906): 295–301

Philander S G H. 1985. El Niño and La Niña. J Atmos Sci, 42(23): 2652–2662

Philander S G H, Fedorov A. 2003. Is El Nino sporadic or cyclic? Annu Rev Earth Planet Sci, 31: 579–594

Picaut J, Masia F, du Penhoat Y. 1997. An advective-reflective conceptual model for the oscillatory nature of the ENSO. Science, 277(5326): 663–666

Rasmusson E M, Carpenter T H. 1982. Variations in tropical sea surface temperature and surface wind fields associated with the southern oscillation/El Niño. Mon Wea Rev, 110(5): 354–384

Rayner N A, Parker D E, Horton E B, et al. 2003. Global analyses of sea surface temperature, sea ice, and night marine air temperature since the late nineteenth century. J Geophys Res, 108(D14): doi: 10.1029/2002JD002670

Suarez M J, Schopf P S. 1988. A delayed action oscillator for ENSO. J Atmos Sci, 45(21): 3283–3287

Sun Hongchuan, Zhou Guangqing, Zeng Qingcun. 2012. Assessments of the climate system model (CAS-ESM-C) using IAP AGCM4 as its atmospheric component. Chinese Journal of Atmospheric Sciences (in Chinese), 36(2): 215–233

Trenberth K E. 1997. The Definition of El Niño. Bull Amer Meteor Soc, 78(12): 2771–2777

Weisberg R H, Wang Chunzai. 1997. A western Pacific oscillator paradigm for the El Niño-Southern Oscillation. Geophys Res Lett, 24(7): 779–782

Wu Bo, Li Tim, Zhou Tianjun. 2010. Asymmetry of atmospheric circulation anomalies over the western north Pacific between El Niño and La Niña. J Climate, 23(18): 4807–4822

Wyrtki K. 1975. El Niño-The dynamic response of the Equatorial Pacific Ocean to atmospheric forcing. J Phys Oceanogr, 5(4): 572–584

Xue Feng, He Juanxiong. 2007. The influence of the extratropical atmospheric disturbances on ENSO. Chinese Journal of Geophysics, 50(5): 1130–1138

Xue Feng, Liu Changzheng. 2008. The influence of moderate ENSO on summer rainfall in eastern China and its comparison with strong ENSO. Chinese Science Bulletin, 53 (5): 791–800

Yu J Y, Kim S T. 2010. Identification of central-Pacific and eastern-Pacific types of ENSO in CMIP3 models. Geophys Res Lett, L15705, doi: 10.1029/2010GL044082

Zebiak S E, Cane M A. 1987. A model El Niño-Southern Oscillation. Mon Wea Rev, 115(10): 2262–2278

Zhang He. 2009. Development of IAP atmospheric general circulation model version 4.0 and its climate simulations [dissertation]. Beijing: University of Chinese Academy of Sciences, 194

Zhou Guangqing, Li Chongyin. 1999. Simulation on the relation between the subsurface temperature anomaly in western Pacific and ENSO by using CGCM. Climatic and Environmental Research (in Chinese), 4(4): 346–352

Zhou Guangqing, Zeng Qingcun, Zhang Ronghua. 1999. An improved air-sea coupled model and its numerical simulation. Progress in Natural Science (in Chinese), 9(6): 542–551